European Journal of Mechanics B/Fluids 29 (2010) 43–52

Contents lists available at ScienceDirect

European Journal of Mechanics B/Fluids

journal homepage: www.elsevier.com/locate/ejmflu

Dynamic interaction of fixed dual spheres for several configurations and inflow conditions

A. Jadoon [a], L. Prahl [b], J. Revstedt [a,*]

[a] Div. of Fluid Mechanics, Lund University, SE-221 00 Lund, Sweden
[b] Dept. of Mechanics, Royal Institute of Technology, SE-100 44 Stockholm, Sweden

ARTICLE INFO

Article history:
Received 3 July 2008
Received in revised form
16 September 2009
Accepted 22 September 2009
Available online 2 October 2009

Keywords:
Particle interactions
Volume of Solid (VOS)
Wake structures

ABSTRACT

The changes in force characteristics as well as the shedding patterns for various dual sphere configurations are studied. The Reynolds numbers considered are 300, 600 and two different inflow conditions are used: steady and pulsating. The sphere formations are defined by the separation distance D_0 between the spheres and the angle between the line connecting the centres of the spheres and the main flow direction, γ. The position of one of the spheres is varied in the range 0°–90° using a 15° increment. Two separation distances are studied; 1.5D and 3D. The method used for the simulations is the Volume of Solid (VOS) approach, a method based on Volume of Fluid (VOF). A major conclusion from this work is that the sphere interaction alters the wake dynamics by obstructing the vortex shedding (generating a steady wake or a wake with lower Strouhal number) and by changing the direction of the lift force so that it in most cases is directed in the plane containing the sphere centres. The results also show that changing the inflow condition gives the same relative change in drag and lift as for a single sphere. The drag is substantially reduced by placing the sphere downstream in a tandem arrangement and slightly increased in a side-by-side arrangement. However, the effect is decreased by increasing separation distance and increasing Reynolds number.

1. Introduction

The flow around a single particle has been vastly investigated throughout literature [1–4]. In a uniform flow, the flow past a single sphere at low Reynolds numbers is attached and steady. As the Reynolds number reaches a value of about 20, the boundary layer separates from the sphere and a steady vortex ring is formed [5,2]. The wake downstream the sphere is extended as the Reynolds number is increased, but remains axis-symmetric until $Re = 210$–212 [2,5–7]. At this Reynolds number, a regular bifurcation has been observed at which the wake is transformed into a planar symmetric wake. However, the flow remains steady until the Reynolds number reaches a value of about 270. Natarajan and Acrivos [6] reported a threshold value of 277.5 while Tomboulides and Orszag [7] on the other hand observed this transition to occur in the interval $Re = 270$–285 and Johnson and Patel [2] predicted a value within the range $Re = 270$–280. The bifurcation connected to this transition (where the steadiness of the wake is lost) has been identified as a Hopf bifurcation. Instead the flow now exhibits time periodicity and planar symmetry is found around. A single dominant vortex shedding frequency of $St = 0.137$ for $Re = 300$ was identified by Johnson and Patel [2] and Tomboulides and Orszag [7]. Further increasing the Reynolds number leads to a chaotic flow where the planar symmetry is lost for $Re = 300$–500 [7]. Sakamoto and Haniu [8,9] reported this transition to occur for $Re > 420$. On the other hand, Gushchin and Matyushin [10] and Mittal et al. [11] observed the wake to loose its planar symmetry at $Re = 375$ and $Re = 360$, respectively. Moreover, Mittal et al. [11] reported the loss of planar symmetry was not immediately followed by the appearance of statistically axi-symmetric wake. Instead the wake undergoes a transition at which the vortex loops are formed at preferred orientations ($Re = 500, 650$). The presence of preferred orientations becomes less significant as the Reynolds number is increased and the wake approaches a statistically axi-symmetric state ($Re = 1000$). As for the vortex shedding, Gushchin and Matyushin [10] explained three different vortex formation mechanisms behind a sphere in the range of $200 < Re < 380$.

Considering the interaction among spheres, studies of the unsteady periodic (based on single sphere observation i.e. $Re > 285$) and chaotic regime ($Re > 380$) are scarce. For these higher Reynolds numbers, more work is required to fully understand the effects of the presence of an additional sphere on the flow field, wake structure, shedding frequencies as well as the interaction among the spheres. Both experimental and numerical work has been carried out, most

* Corresponding author. Tel.: +46 46 222 4302; fax: +46 46 222 4717.
E-mail address: johan.revstedt@energy.lth.se (J. Revstedt).

0997-7546/$ – see front matter © 2009 Elsevier Masson SAS. All rights reserved.
doi:10.1016/j.euromechflu.2009.09.003

common are the tandem and side-by-side formations, i.e. the line joining the centres of the spheres is perpendicular to the flow direction, to investigate the effect of separation distances on the particles drag, lift and momentum coefficients [12–16]. For sphere arrangement considering other formations than those mentioned above, Olsson and Fuchs [17], Chen and Wu [18] and Prahl et al. [19] all considered the effect of the inclusion of a second sphere as the relative position in-between the spheres was changed, i.e. positioning a secondary sphere around a reference sphere at an angle to the main flow direction. These studies were all carried out in the steady axi-symmetric range, i.e. for $Re < 200$. Formations including more than two spheres have been studied by Chen and Lu [20], Tsuji et al. [21] and Liang et al. [22].

In all the above mentioned studies, the importance of the separation distance is pointed out which in turn significantly affects the drag, lift and shedding patterns. Generally for side-by-side arrangements at moderate Reynolds numbers, the drag increases with a decrease in separation distance. Regarding small distances when the particles are almost in contact at relatively low Reynolds numbers (100), several studies have reported the flow to consider the spheres as a single body due to a blockage effect [13,17,21]. Regarding flow at $Re = 300$, Schouveiler et al. [15] observed an out-of-phase shedding for smaller separation distances. For intermediate separation distance, two wakes with in-phase shedding were reported and for large separation distance the shedding from each sphere was independent of the other. Due to a high-pressure region in front of the secondary (downstream) sphere that interacts with a low-pressure region behind the reference (upstream) sphere, spheres in tandem formation at small distances are subjected to an increase in drag. However, the drag of the reference sphere is still smaller than that an isolated sphere is subjected to. Considering tandem formations, the position of the secondary sphere is the main reason for drag reduction if placed in the wake of the reference sphere [17,23,19]. For Reynolds numbers less than 210, spheres in tandem formation are not subjected to any lift force. However, as the Reynolds number is increased to 300, the wake transforms from being steady and axi-symmetric to steady and plane symmetric to unsteady as the separation distance is increased from 1.5 to 2.5D. At a separation distance of 3–4D, the wake undergoes 3D transition; further increasing the separation distance transforms the wake back into a planar symmetry state [16].

The purpose of this paper is to further increase the understanding of the interaction among spheres in the unsteady wake. As a result, the motivation is to improve existing models (Eulerian–Lagrangian) for handling particulate flows. Simulations for single sphere case as well as dual sphere case changing the relative position among the spheres are carried out in order to investigate the effect a second sphere will have on the force characteristics as well as the shedding frequencies. Two different inflow conditions are applied: steady and pulsating, and the Reynolds number studied are $Re = 300$ and $Re = 600$. The reason for including a time dependent inflow is to be able to investigate how the wake and the forces respond to flow unsteadiness and thereby move closer to understanding how particles would behave in a turbulent environment.

2. Numerical method

$$\frac{\partial u_i}{\partial x_i} = 0 \tag{1}$$

$$\frac{\partial u_i}{\partial t} + u_j\frac{\partial u_i}{\partial x_j} = -\frac{\partial p}{\partial x_i} + \frac{1}{Re}\frac{\partial^2 u_i}{\partial x_j^2} \tag{2}$$

The continuity and momentum equations, (1) and (2), governing an isothermal, incompressible flow of a Newtonian fluid are spatially discretised using first and second order basic finite-difference schemes on a staggered Cartesian grid. The Cartesian staggered grid consists of orthogonal hexahedral shaped cells at which the dependent variables are positioned at different points of the computational cell i.e. the velocity components at the cell faces and the pressure in the cell centre. Staggered grids have the advantage of preventing pressure oscillations. A single step defect correction method [24] is used to improve the accuracy to third order for convective terms and fourth order for remaining terms without losing numerical stability. A second order fully implicit scheme is used for temporal discretisation. In order to enhance the computational efficiency a multi-grid method is used within each time step. The pressure–velocity coupling is done through simultaneous update of dependent variables as the continuity equation is relaxed [25].

2.1. Volume of solid (VOS)

The volume of solid (VOS) method [26] is based on the VOF approach in which amount of the fluid and solid in each cell is defined. In VOS the shear stress is assumed to be constant because of the dominant viscous forces near the surface, thus the 'second fluid' can be assumed to be with infinite viscosity. In the VOF approach [27,28], assuming linear relationship between amount of fluid in a cell and average viscosity of that cell, from which the viscosity factor can be defined as:

$$\mu = (1-\alpha)\mu_1 + \alpha\mu_2 \tag{3}$$

where μ_1 and μ_2 are the viscosity factors of the two fluids. Assuming constant shear stress near the interface, a similar relation for the viscosity factor can be written:

$$\mu = \frac{1}{\frac{\alpha}{\mu_1} + \frac{1-\alpha}{\mu_2}} \tag{4}$$

As mentioned above the shear stress is nearly constant due to viscosity dominance near the boundaries, Eq. (4) is therefore used in the VOS method. Regarding solids (the second fluid), the viscosity is infinite leading to a simple relation where α is the phase variable representing the amount of fluid in each cell, $0 < \alpha < 1$. Cells containing only solid phase will be blocked as there will be no flow ($\alpha = 0$) in these cells. Thus no computation will be carried out for these cells. The VOS method was shown by Lörstad [29] to be second order accurate. Further details regarding this technique can be found in the work by Lörstad and Fuchs [26].

Assuming constant density, the ratio of kinematic viscosity $\delta\nu$ can be expressed as

$$\delta\nu = \frac{\nu}{\nu_1} = \frac{\mu}{\mu_1} = \frac{1}{\alpha} \tag{5}$$

With the definition of viscosity term as stated in Eq. (5), the governing equations for an incompressible flow can be written as:

$$\frac{\partial u_i}{\partial x_i} = 0 \tag{6}$$

$$\frac{\partial u_i}{\partial t} + u_j\frac{\partial u_i}{\partial x_j} = -\frac{\partial p}{\partial x_i} + \frac{1}{Re}\frac{\partial}{\partial x_j}\left(\delta\nu\left[\frac{\partial u_i}{\partial x_j} + \frac{\partial u_j}{\partial x_i}\right]\right) \tag{7}$$

By integrating the momentum equations over a control volume and then transforming the volume integral to surface integral using Gaussian theorem the following equation is obtained:

$$F_i = \iiint_{\Omega} \frac{\partial u_i}{\mathrm{d}t}\mathrm{d}\Omega + \iint_{\Gamma}\left(u_i u_j n_j + p n_i - \frac{1}{Re}\left[\frac{\partial u_i}{\partial x_j} + \frac{\partial u_j}{\partial x_i}\right] n_j\right)\mathrm{d}\Gamma \tag{8}$$

where Γ represents the outer surface of a control volume and n is the unit vector normal to the surface. The forces acting on the object is obtained by applying Eq. (8) on the faces of the cube (control volume is created here by subtracting the object from cubical box). Note that $\alpha = 1$ on the surface Γ, therefore $\delta\nu = 1$ is omitted from Eq. (8).

3. Problem set-up

In this study, two equally sized spheres with a diameter D are held fixed in a rectangular domain while changing the relative position between the spheres, Fig. 1. The sphere positions are defined by the separation distance D_0 and the angle γ between the line connecting the centres of the spheres and the main flow direction. Simulations are carried out for $D_0 = 1.5$ and $3D$, γ is varied from 0° to 90° using 15° increment. We denote the sphere which is affected by the presence of another sphere *secondary sphere* and the sphere used to cause this influence *reference sphere*. Hence, for $0° \le \gamma < 90°$ the data come from the downstream sphere and for the range $90° < \gamma \le 180°$ the upstream sphere is used. The Reynolds numbers considered are 300 and 600. At the inlet, we set either a steady inflow, $U_{\mathrm{in}} = U_0 = 1$, or a flow with a sinusoidal variation around this value, i.e.

$$U_{\mathrm{in}} = U_0 + A_{\mathrm{U}} \sin(2\pi St_{\mathrm{in}} t) \tag{9}$$

The flow is pulsating with amplitude ($A_{\mathrm{U}} = 0.1U_0$), and a Strouhal number of ($St_{\mathrm{in}} = fD/U_{\mathrm{in}}$) of 0.1. These conditions are applied for spheres placed in several separation distances and angular positions.

In order to validate the accuracy of the VOS method, simulations are carried out for a single sphere at $Re = 300$ and 600. A sensitivity study investigating the influence of blockage, distance to the outflow boundary and the grid resolution was performed. The influence of distance to the outflow boundary was investigated for sizes of 16D, 32D and 64D in the stream-wise direction (Z direction), while keeping the dimensions in the X and Y directions fixed at 32D. Similarly, to investigate the area blockage effect (X and Y directions), domain sizes of 16, 24 and 32D were used, keeping the stream-wise direction dimension fixed to 64D. In both cases the change in drag is about 0.27% when increasing the dimension from [32, 32, 32]D to [32, 32, 64]D and [24, 24, 64]D to [32, 32, 64]D for the stream-wise and lateral directions, respectively (Fig. 2(a) and (b)). A domain size of [32, 32, 64]D was used to study the effects of grid resolution. These results are shown in Fig. 2(c), and good agreement with the results of Johnson and Patel [2] and Natarajan and Acrivos [6] was obtained using a mesh size of $h = D/64$. A mesh size of $h = D/64$ and a domain size of [32, 32, 64]D are used in all simulations.

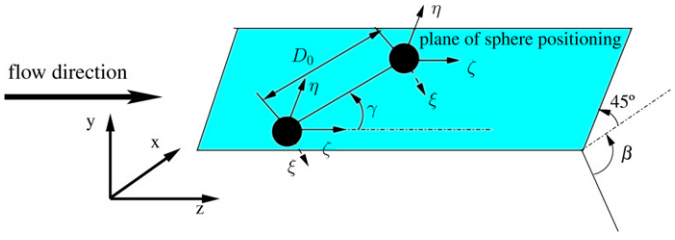

Fig. 1. The computational set-up and coordinate systems.

In all simulations, the single sphere is placed 10D downstream of the inlet and centred in the x–y plane. This is also the position of the upstream sphere in the dual sphere formations. The downstream sphere is positioned in a plane 45° from the x to z plane. A reason being that this will allow a longer distance between the downstream sphere and the outer boundary. To see the direction of the lift with respect to the sphere positioning more clearly the results will be presented in a local coordinate systems aligned with the plane containing the sphere centres and originating from the

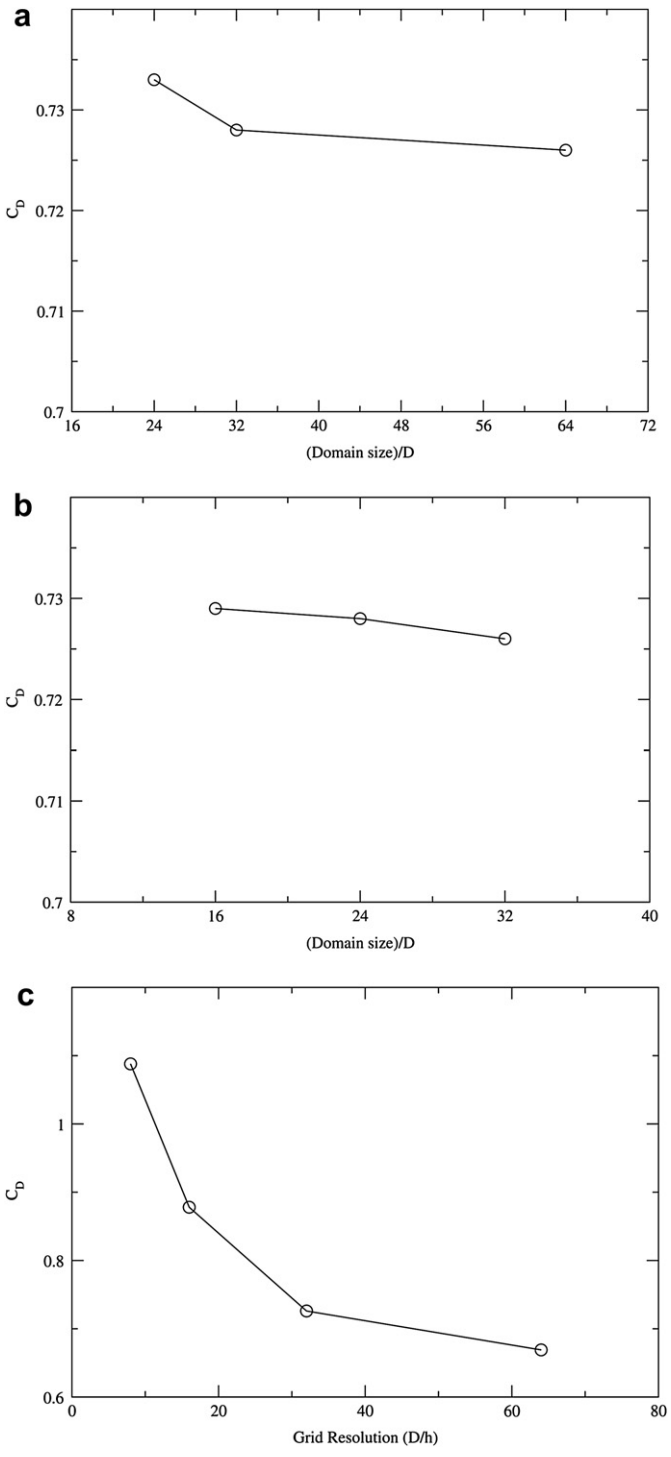

Fig. 2. C_{D} as a function of domain size in stream-wise direction (a), lateral dimensions [x, y] (b) and grid resolution (c).

centre of each sphere. Hence, η is the coordinate in that plane and normal to the main flow direction (z) and ξ is the coordinate normal to the plane containing the sphere centres, see Fig. 1. Also, the direction of the lift force is given by the angle β, where $\beta = 0^\circ$ corresponds to the positive ξ direction.

Throughout the paper, the λ_2-method of Jeong and Hussain [30] is used for vortex visualisation. This technique defines the vortex as any region with negative second eigenvalues of tensors $S^2 + \Omega^2$, where S and Ω are the local rate of strain and rate of rotation tensors, respectively. The drag and lift coefficients for the dual particle cases are normalised by the single sphere values except for the lift coefficient at $Re = 600$ since for this case the time averaged lift coefficient is zero.

4. Results

The wake of a sphere and especially the recirculating part is either axi-symmetric or plane symmetric. By plane symmetric is understood that a well defined plane of symmetry exists in the wake, and that the lift force is parallel to this plane. This is true both for the steady wake and, in a statistical sense, also for the unsteady wake. However, for the unsteady wake plane and axi-symmetry is not sufficient to fully characterise the wake dynamics. Considering the components of the instantaneous lift coefficient, four regimes can be identified for the unsteady wake and in the following we will refer to these as: *unidirectional* for which the lift is varying in magnitude but the direction is always along a line; *cyclic* for which both the direction and the magnitude of the lift coefficient vary periodically; *semi-chaotic* for which the lift has a preferred direction but with a random fluctuation around this direction, *chaotic* for which the variation is random and no preferred direction is present. Note that chaotic does not necessarily imply axi-symmetry.

4.1. Single sphere

In order to better understand the phenomena occurring in dual sphere configurations we first consider the flow situation for a single sphere. The mean values of the force coefficients, the fluctuations thereof and shedding frequency for a single sphere at $Re = 300$ are presented in Table 1. As can be seen, our results, both on force coefficients and shedding frequency, agree well with previous studies [2,7,31,32]. A visualisation of a typical instantaneous vortex pattern for this case is depicted in Fig. 3. Vortices are shed from the sphere periodically and with the same orientation. By considering a phase plot of the lift coefficient components one will find a periodic variation of the lift coefficient but the direction is constant. Hence, this wake is characterised as unidirectional and statistically plane symmetric. Pulsating the inflow with a Strouhal number of 0.1 will decrease the mean drag and lift coefficients slightly. The drag and lift fluctuations, on the other hand, will increase substantially indicating an increased unsteadiness of the wake (Table 1). However, the wake is still unidirectional but with the shedding locked-on to the inflow frequency.

Table 1
Comparison of force coefficients and Strouhal number for single sphere at $Re = 300$.

	St	C_D	ΔC_D	C_L	ΔC_L
Steady inflow	0.138	0.669	0.003	−0.068	0.013
Revstedt [32]	0.131	0.67	0.0024	−0.068	0.012
Johnson and Patel [2]	0.137	0.656	0.0035	−0.069	0.01
Tomboulides and Orszag [7]	0.136	0.671	0.0028	–	–
Ploumhans et al. [31]	0.135	0.683	0.0025	−0.061	0.014
Pulsating inflow	0.1	0.675	0.053	0.056	0.044

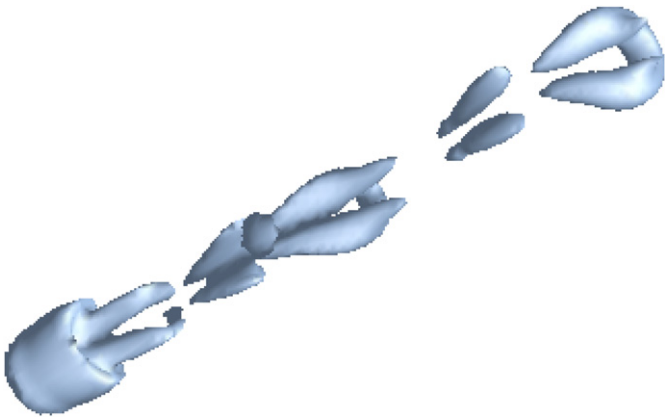

Fig. 3. Diagonal view of the vortical structures behind a single sphere at $Re = 300$, steady inflow.

For $Re = 600$ the drag coefficient is slightly higher for the pulsating inflow, 0.58 compared to 0.56 for the steady case. As the Reynolds number is increased, the transition to a chaotic flow situation through a loss of planar symmetry has been reported to appear at $Re > 375$ by Gushchin and Matyushin [10] and at $Re > 420$ by several authors [8,9,31]. Plotting the time trace of the components of the instantaneous lift C_{Lx} and C_{Ly}, against each other it is clear that the lift has no preferred direction (Fig. 4). A highly complex and irregular pattern is found, which is also shown in the visualisation of an instantaneous vortex pattern in Fig. 5. Furthermore, the mean C_L is zero and the wake can therefore be classified as chaotic and statistically axi-symmetric. This is true for both the steady and the pulsating inflow conditions. However, as for $Re = 300$ the amplitude of the force coefficient fluctuations is larger for the pulsating inflow although the difference is smaller for $Re = 600$. Furthermore, there is a very low frequency variation present which in the steady inflow case is found at a Strouhal number, $St \approx 3 \times 10^{-3}$, and for the pulsating flow at $St \approx 8 \times 10^{-3}$. By using proper orthogonal decomposition (POD) Prahl et al. [33] found that this frequency is connected to an axial instability mode in the wake, which cannot be observed for the pulsating inflow. The above is in agreement with the results of Sakamoto and Haniu [8,9],

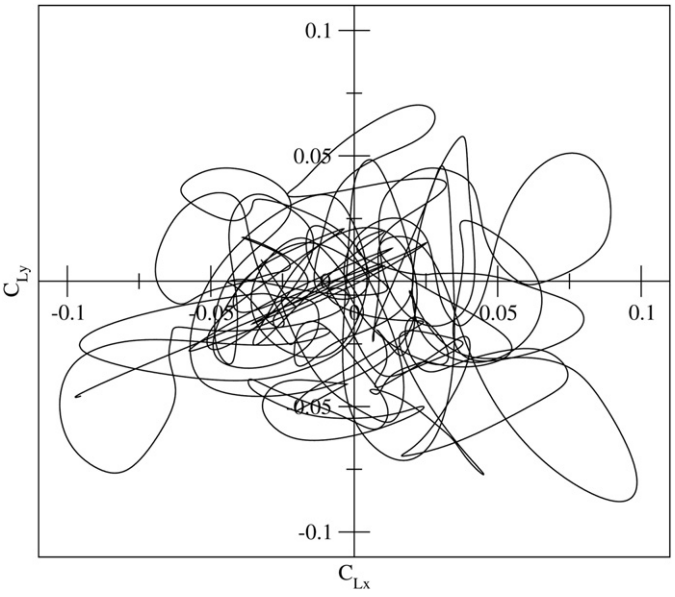

Fig. 4. Phase plot for single sphere at $Re = 600$, steady inflow.

Fig. 5. *yz* view of the vortical structures behind single sphere at $Re = 600$, steady inflow with flow direction from left to right.

who also reported the shedding pattern of vortex loops in irregular mode with no definite point of shedding of hairpin-shaped vortices. However, Mittal et al. [11] found the flow to be plane symmetric with a preferred orientation of the vortex loops at $Re = 650$. We also find this initially (which can be seen in Fig. 4) but as the flow develops in time the flow transforms into the chaotic and statistically axi-symmetric state. Due to the chaotic character of the wake it is more difficult to find a clear shedding frequency at $Re = 600$. However, from the spectra of the lift coefficient components we find that $St = 0.1$ is dominating both for steady and pulsating inflow. As stated earlier the position of the vortex shedding is moving around the circumference of the sphere, which might be the origin of low frequency components of the lift coefficient.

4.2. Dual spheres

4.2.1. $Re = 300$

Previous studies of sphere interactions performed at lower Reynolds numbers [17,19] ($Re \leq 200$) show that the drag coefficient will be reduced on both spheres in almost all configurations except if the angle towards the flow direction is close to 90°. In that case a slight increase in drag coefficient occurs if the distance between spheres is less than 2*D*. These studies also show that the interaction will give rise to a lift force due to the redirection of the wakes. Also, the maximum distance for which the lift force is detected increases with increasing Reynolds number [19]. Hence, one may suspect that at the Reynolds numbers considered in the present work there are two competing effects for generating lift, the sphere interaction and the wake asymmetry.

Positioning the secondary sphere in a downstream tandem position, i.e. $\gamma = 0°$, one would expect a substantial decrease in mean drag coefficient since it will be in wake of the reference sphere. As can be seen from Fig. 6 at a separation distance $D_0 = 1.5D$ the drag on the secondary sphere is about 18% of the value for a single sphere. Increasing the distance to $D_0 = 3D$ the drag increases to about 50% of the single sphere value. Also note that for a pulsating inflow the value is 60% which can probably be explained by that the recirculation zone of the reference sphere is somewhat shorter in this case (1.7*D* as compared to 1.9*D* for a steady inflow), which in turn leads to higher velocities on the wind-ward side of the secondary sphere.

Moving the secondary sphere out of the reference sphere wake, i.e. increasing γ, the drag is of course increased since more of the oncoming flow will directly hit it. Already at $\gamma = 15°$ and $D_0 = 1.5$ the drag has increased to 80% of the single sphere value and a continuous increase in drag is observed until $\gamma = 120°$ (110%) where after it again decreases. At $\gamma = 180°$ (i.e. tandem arrangement with the secondary sphere in the upstream position) the drag is slightly below that of a single sphere. The same trend is found for a separation distance of 3*D*, however the influence is lower. Also note that changing the inflow boundary condition only has a marginal effect on the mean drag coefficient. For all angular positions and at both separation distances considered in this work the fluctuations in drag coefficient are lower than for the single sphere case. Only in side-by-side arrangement they are comparable in magnitude to the single sphere case. This suggests that the reference sphere will have a damping effect on the wake fluctuations, which is discussed further below.

Turning our attention to the mean lift coefficient we find a more complex behaviour. Fig. 7 depicts the absolute value of the mean lift coefficient on the secondary sphere as a function of angular position for both separation distances. At $\gamma = 0°$ (downstream tandem) the lift coefficient is zero for the steady inflow condition which is also true for the upstream tandem formation. Hence, in this arrangement the wake asymmetry cannot develop resulting in an axi-symmetric wake. Again, as the secondary sphere is moved out of the reference sphere wake it is directly influenced by the oncoming flow and immediately one will observe an increase in mean lift coefficient, which is due to a skewness in the wake caused by the redirected flow in the gap between the spheres. This is clearly seen in Fig. 8a showing the averaged flow field in the plane of the lift force for $\gamma = 15°$ and $D_0 = 1.5$. A local minimum in lift

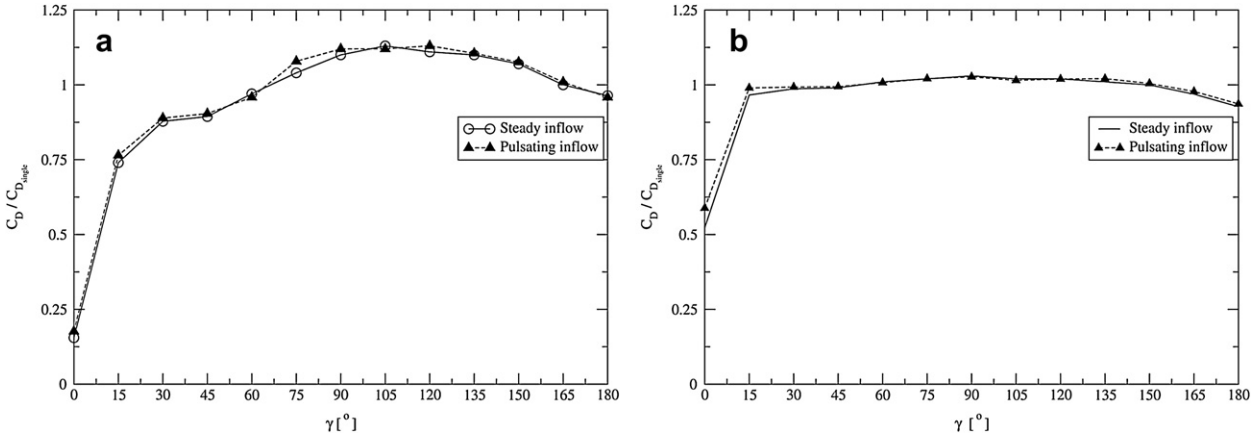

Fig. 6. C_D as function of angular position γ a separation distances of 1.5*D* (a) and 3*D* (b) at $Re = 300$. Both steady and pulsating inflow.

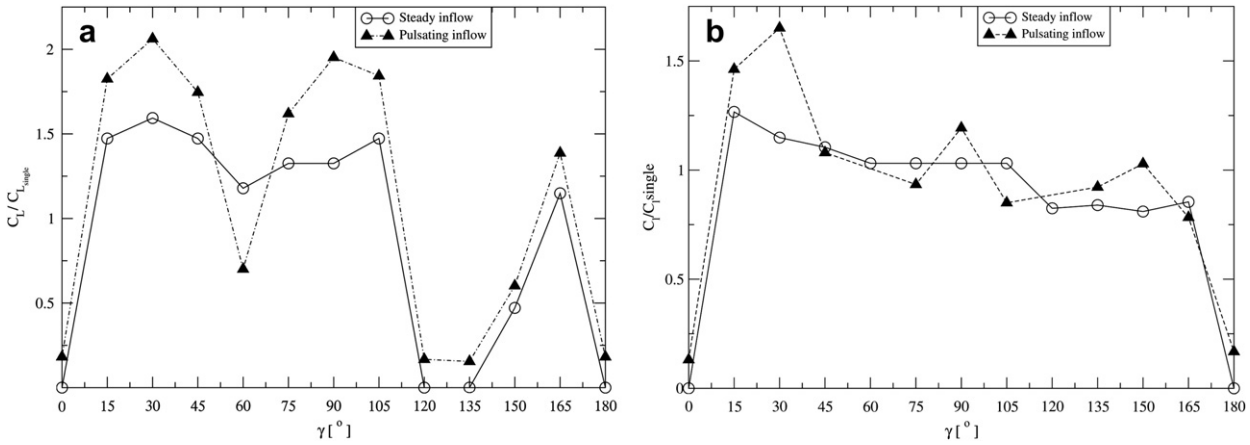

Fig. 7. Absolute value of mean C_L as function of angular position γ at $D_0 = 1.5D$ (a) and $D_0 = 3D$ (b) for $Re = 300$. Both steady and pulsating inflow.

coefficient is found at $\gamma = 60^\circ$ which can be explained by that somewhere between 45° and 60° the lift force changes direction. This change from attraction to repulsion and the change back to attraction between $\gamma = 120^\circ$ and $\gamma = 135^\circ$ can clearly be seen by observing the change in wake asymmetry between Fig. 8b and d, i.e the changing position of the wake vortex. Yoon and Yang [34] also noted the presence this change in vortex shedding angle for separation distances up to 6*D*.

Also note that pulsating the inflow leads to larger lift coefficient. Increasing the separation distance to 3*D* changes the behaviour of the lift coefficient. At the tandem formations the value is still zero in the steady inflow case, indicating an axi-symmetric wake. For all other formations C_L is only varying slightly with a maximum at $\gamma = 15^\circ$. It also interesting to note that the "natural" plane symmetric wake behaviour does not develop for any angular position for steady inflow at $Re = 300$. This is shown by the fact that

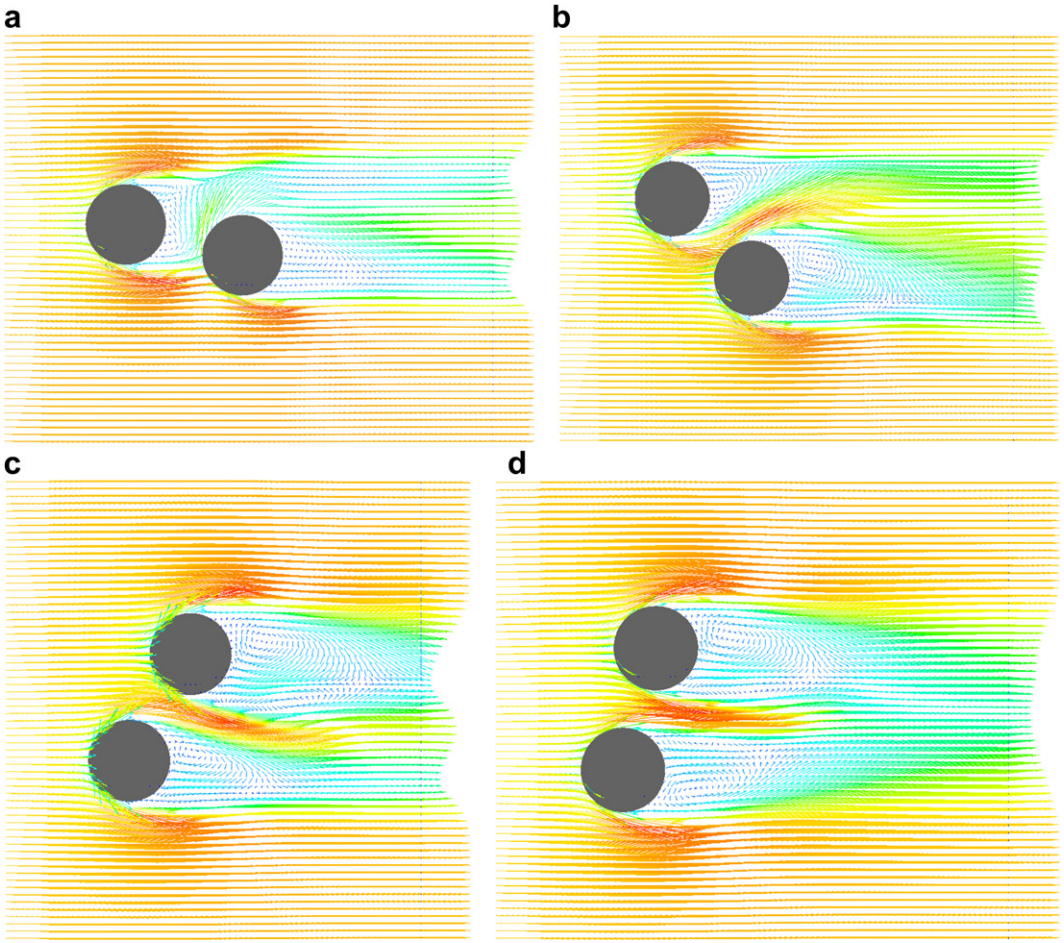

Fig. 8. Mean velocity fields in the η–z plane for steady inflow and $Re = 300$ at 15° and 165° (a), 45° and 135° (b), 60° and 120° (c) and 75° and 105° (d).

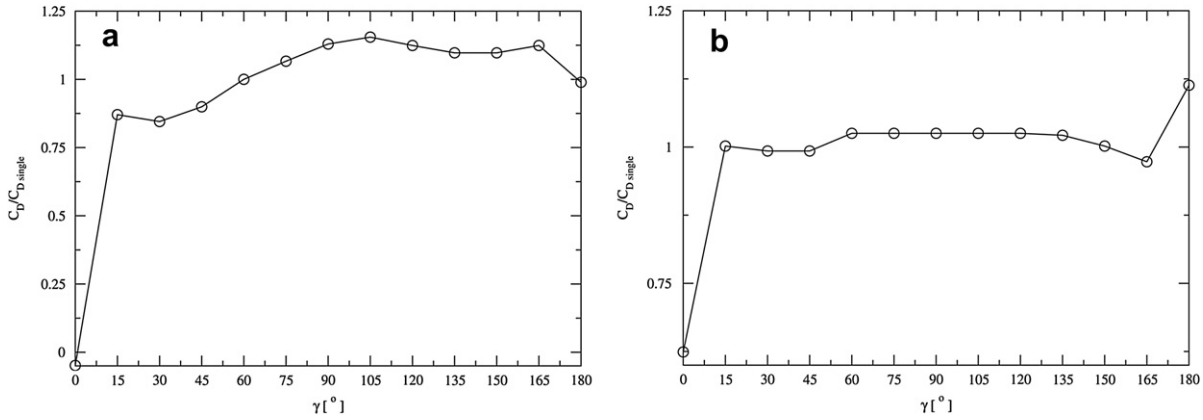

Fig. 9. C_D as function of angular position γ at separation distances of 1.5D (a) and 3D (b) at $Re = 600$, steady inflow.

the lift force is in almost all cases oriented in or very close (a deviation of up to 5°) to the plane containing the sphere centres (i.e. in the η direction which corresponds to $\beta = 90°$) whereas in the single sphere case the plane containing the lift force is oriented at 25° from this plane. However, some positions deviate from this pattern. At $\gamma = 120°$ the direction of lift is at $\beta = 53°$ for $D_0 = 1.5$ and at $\beta = 78°$ for $D_0 = 3D$ for the steady inflow case. It seems that as the lift is changing direction from repulsion to attraction the wake is not flipped but rather rotated around the ζ-axis. The same effect is also observed for the pulsating inflow case and at the direction change between 45° and 60°. However, at these angles the effect is much weaker.

The Strouhal number of vortex shedding for a single sphere in steady inflow at $Re = 300$ is, as mentioned above, just below 0.14 and pulsating the inflow the shedding will be locked-on to the Strouhal number of the inflow (0.1). Introducing a second sphere does not change this, generally. Although there are some exceptions. For $D_0 = 1.5D$ the secondary sphere will have a strong effect on the wake in the positions close to tandem (i.e. $0° \leq \gamma \leq 30°$ and $150° \leq \gamma \leq 180°$). At these positions the sphere interaction will have a stabilising effect which leads to a steady wake. In tandem position the wake is also axi-symmetric. At all other positions the shedding will have the same Strouhal number as for the single sphere. However, due to the interaction of vortices shed by the upstream cylinder with the downstream cylinder wake harmonics of the shedding frequency are more pronounced than in the single sphere case. Still the wake can for these cases be characterised as unidirectional and plane symmetric as in the single sphere case. Increasing the separation distance to 3D the wake is unsteady for all angles and the shedding frequency is close to the single sphere value except at tandem formation where the damping effect leads to a lower Strouhal number (0.1). Here the wake is also unidirectional at all angles and statistically plane symmetric except in tandem where it is axi-symmetric. For the pulsating inflow the trend is the same as for steady inflow except that the wakes have a cyclic character instead. Of course the wake is unsteady at all angles here but as for the steady inflow case shedding is obstructed at angles close to tandem formation. The frequency for all cases is the same as for single sphere (0.1) except at $\gamma = 90°$ and $D_0 = 1.5$ where also the natural shedding frequency is observed.

4.2.2. $Re = 600$

Increasing the Reynolds number to 600 it is evident from Fig. 9 that these cases show the same trend for C_D as for $Re = 300$ when varying the angular position. However, the drag reduction is much stronger at $D_0 = 1.5D$ in the downstream tandem formation (Fig. 9a). In fact the effect is so strong that the sphere embedded in the wake experiences a negative drag. At $D_0 = 3D$ (Fig. 9b) the drag reduction is, as expected, much less pronounced except at the upstream tandem formation where the drag is actually increased to about 110% of the single sphere value. This is probably an effect of the change in wake structure occurring at this formation, which is discussed further below. In the single sphere case the mean lift is zero since the wake is statistically axi-symmetric. Placing spheres 1.5D apart will generate a mean lift for all angular positions. From Fig. 10 one can again observe that the variation of the absolute value

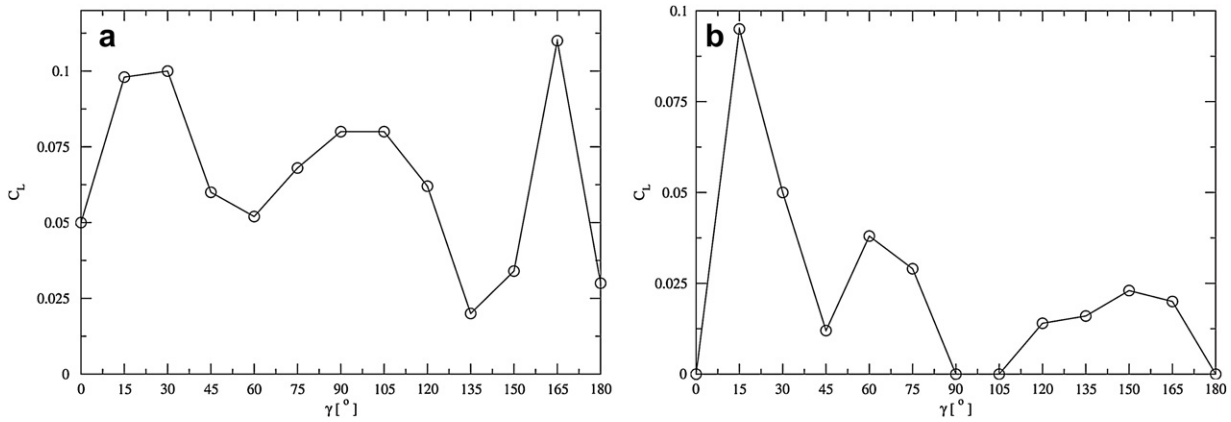

Fig. 10. Absolute value of mean C_L as function of angular position γ at separation distances of 1.5D (a) and 3D (b) at $Re = 600$, steady inflow. Note that C_L in these graphs is not normalised since $C_L = 0$ for single sphere.

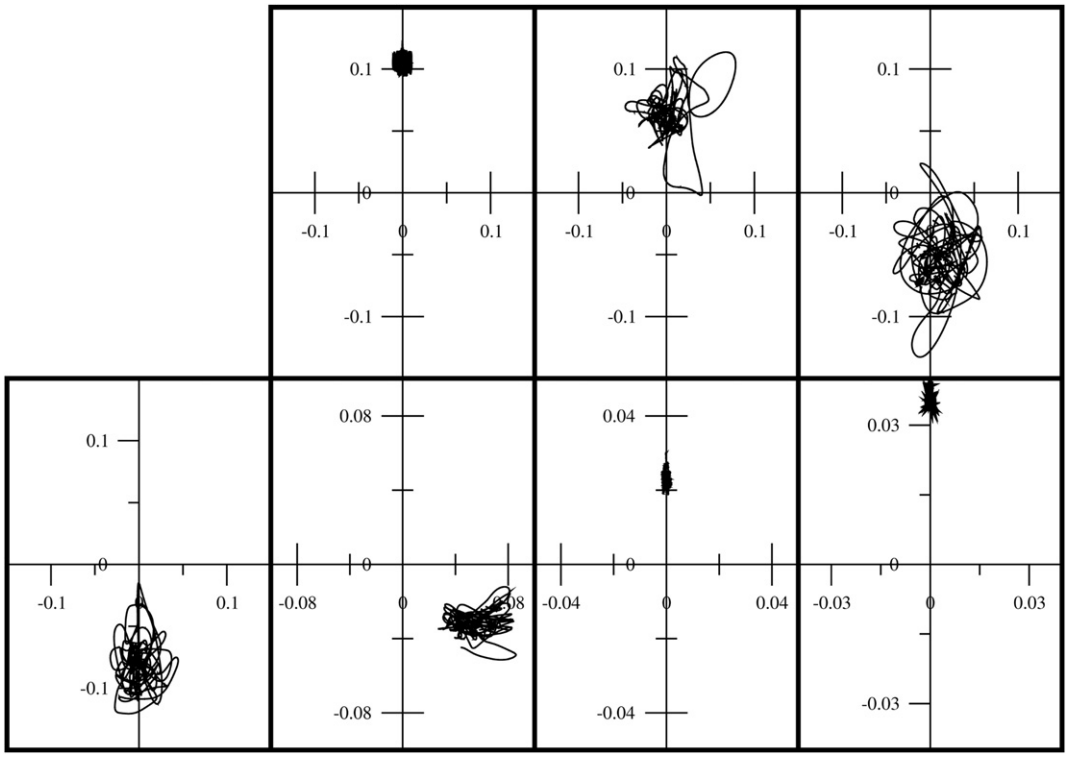

Fig. 11. Phase plot of the lift coefficient at $D_0 = 1.5D$ and $Re = 600$ for several angular positions.

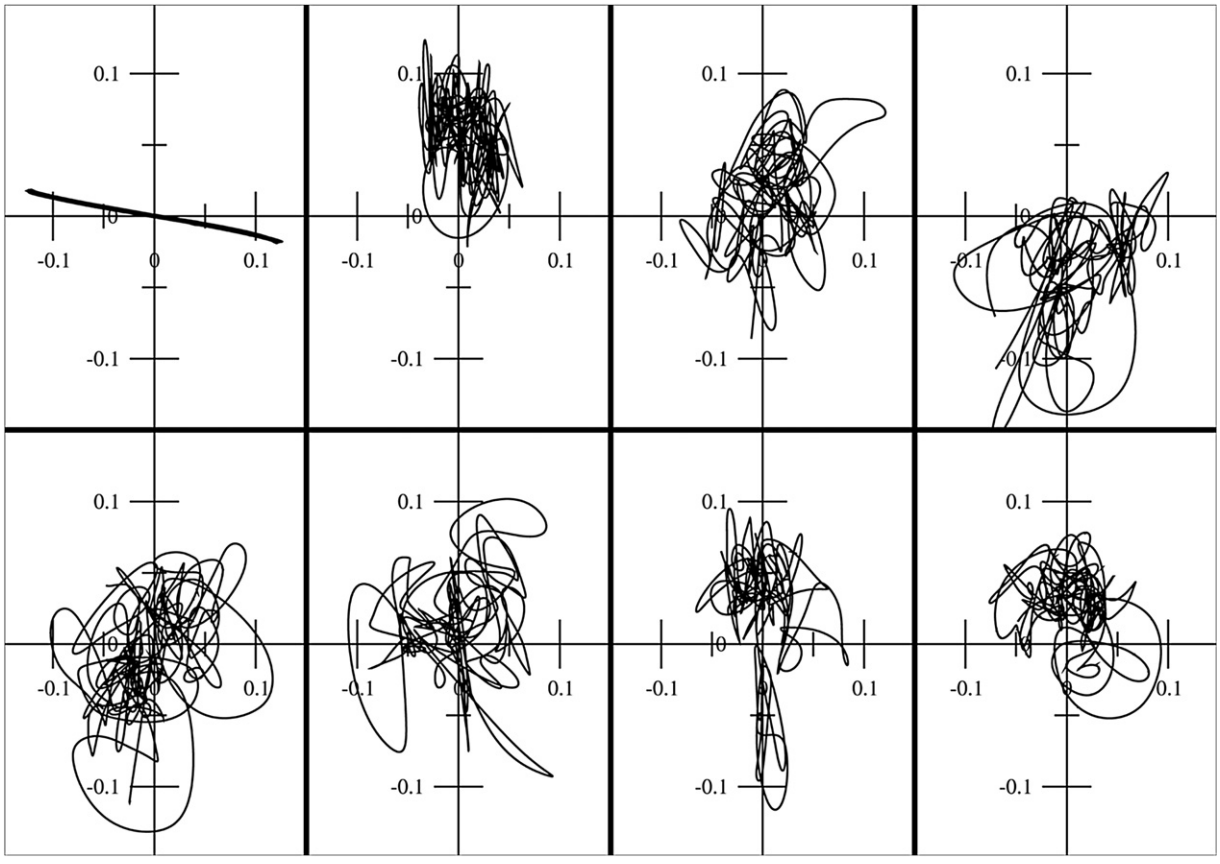

Fig. 12. Phase plot of the lift coefficient at $D_0 = 3D$ and $Re = 600$ for several angular positions.

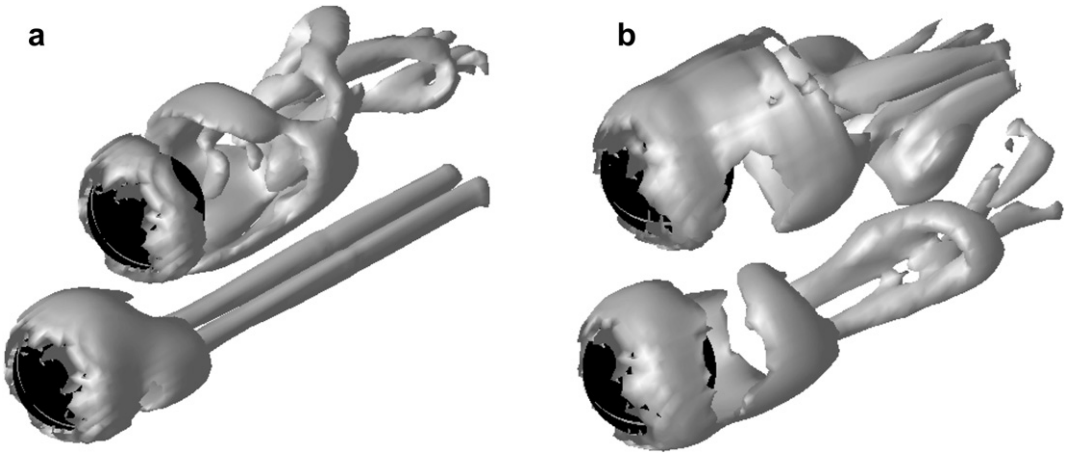

Fig. 13. λ_2 visualisation of the instantaneous wake structure for the angular positions 45° and 135° (a), and 60° and 120° (b) at $D_0 = 1.5D$ and $Re = 600$.

of the mean lift is similar to what was found for $Re = 300$ above, however at no position does the wake become axi-symmetric. At the larger separation distance the behaviour differs more from what is found for the lower Reynolds number. This can be explained by the much stronger effect on the wake dynamics found for $Re = 600$.

To further characterise the wake dynamics caused by the sphere interactions we consider phase plots of the lift coefficient components ($C_{L,\xi}$ and $C_{L,\eta}$). Some characteristic phase plots are shown for $D_0 = 1.5D$ in Fig. 11 and for $D_0 = 3D$ in Fig. 12. At $D_0 = 1.5D$ the sphere interaction is such that the wake is steady in the tandem positions. Moving away from the downstream tandem case the wake becomes unsteady already at $\gamma = 15°$ and since the lift is non-zero for all angles away from the tandem configurations the wake can be considered as statistically plane symmetric. Considering again the temporal development of the lift we find that the character develops from being unidirectional ($\gamma = 15°$) over semi-chaotic ($\gamma = 30°$) to chaotic at $\gamma = 45°$. It will hold this character until $\gamma = 120°$, i.e. in the range of positions where either the oncoming flow is relatively unaffected by the reference sphere wake or where the reference sphere position does not interfere with the wake development. Thereafter, as the upstream tandem position is approached the wake will go back towards the unidirectional character due to the damping effect of the reference sphere. Fig. 13a shows a λ_2 visualisation of the wake vortices for a sphere pair at 45° and 135°. Here one can clearly see the chaotic character of the downstream (45°) sphere wake and how the wake fluctuations are almost totally damped for the upstream sphere (135°). Note however that also at this Reynolds number we have a strong deviation of the direction of the lift from the plane containing the sphere centres at $\gamma = 120°$. Considering Fig. 13b one can clearly see how the orientation of the vortices shed from the upstream sphere causes the lift to fluctuate mainly in the ξ-direction.

The situation at $D_0 = 3D$ is somewhat different. Since the separation distance is longer the wake will have larger possibility to develop. This is reflected by that at the tandem positions the wake is unidirectional and that the chaotic character is visible already at $\gamma = 30°$ and this character is retained up to $\gamma = 165°$. Also, as can be seen in Fig. 10b, close to $\gamma = 90°$ the wake is statistically axi-symmetric which suggests that at this position the sphere interaction is very weak and can only be observed as a slight increase in drag coefficient (Fig. 9b).

5. Conclusions

A pair of spherical particles placed in close proximity will interact and affect each other. Previous studies have considered this interaction in a range of Reynolds numbers where the sphere wake is steady and the interaction is only affecting the forces acting on the spheres. However, considering higher Reynolds numbers, ranging from where the wake is unsteady but orderly ($Re = 300$) to where it starts to be chaotic ($Re = 600$) also the wake dynamics are affected by the interaction potentially changing both the intensity and the character of the wake. The main conclusions from this work may be summarised as:

- Positioning spheres in tandem or close to tandem so that the wakes are strongly affected will lead to a stabilisation such that the wake either becomes steady or unsteady with a lower Strouhal number. Also, the character of the wake dynamics will be changed in such a way that the wake fluctuations will be more ordered. Hence, it will, in this respect, behave as if the Reynolds number was lowered.
- The drag force is affected mainly for a sphere placed in a downstream tandem position where it is significantly decreased and can even be negative. However, for a sphere in the upstream tandem position the drag increase or decrease can be up to 10% of the single sphere value.
- The wake asymmetry observed for a single sphere at $Re = 300$ is also present in the tandem cases when the wake is unsteady. However in most of the other cases the lift force is only slightly deviating from the line connecting the sphere centres, indicating that the interaction between the spheres is totally dominating the lift direction. Also, as the sphere is moved from downstream to upstream tandem the lift force changes direction from attraction to repulsion and back to attraction which also causes the direction of lift to deviate from the inter-sphere direction at the changing locations.
- Pulsating the inflow on a pair of spheres will have approximately the same effect on lift and drag as for a single sphere, i.e. the magnitudes are increased with approximately the same magnitude as in the single sphere case. Also, the wake character is somewhat changed due to the pulsation. In the steady inflow cases the wakes are characterised as unidirectional indicating that the shedding originates from a fixed location on the sphere surface. However, pulsating the inflow will give the wakes a cyclic character indicating a low frequency motion of the point of shedding.

Acknowledgements

The financial support for this work by the Swedish Research Council (Vetenskapsrådet) and the Centre for Combustion Science

and Technology (CECOST) is gratefully acknowledged. Computational resources were provided by the Swedish National Infrastructure for Computing (SNIC) and the Centre for Scientific Computing at Lund University (LUNARC).

References

[1] B. Fornberg, Steady viscous flow past a sphere at high reynolds numbers. J. Fluid Mech. 190 (1988) 471–489.
[2] T.A. Johnson, V.C. Patel, Flow past a sphere up to a reynolds number of 300. J. Fluid Mech. 378 (1999) 19–70.
[3] Kim, J. Pearlstein, Stability of the flow past a sphere. J. Fluid Mech. 211 (1990) 73–93.
[4] S. Lee, A numerical study of the unsteady wake behind a sphere in a uniform flow at moderate Reynolds numbers. Comput. Fluids 29 (2000) 639–667.
[5] S. Taneda, Experimental investigation of the wake behind a sphere at low Reynolds number. J. Phys. Soc. Jpn. 11 (1956) 1104–1108.
[6] R. Natarajan, A. Acrivos, The instability of the steady flow past spheres and disks. J. Fluid Mech. 254 (1993) 323–344.
[7] G. Tomboulides, S.A. Orszag, Numerical investigation of transitional and weak turbulent flow past a sphere. J. Fluid Mech. 416 (2000) 45–73.
[8] H. Sakamoto, H. Haniu, A study on vortex shedding from spheres in a uniform flow. Trans. ASME J. Fluids Eng. 112 (1990) 386–392.
[9] H. Sakamoto, H. Haniu, The formation mechanism and shedding frequency of vortices from a sphere in a uniform shear flow. J. Fluid Mech. 287 (1995) 151–171.
[10] V.A. Gushchin, R.V. Matyushin, Vortex formation mechanisms in the wake behind a sphere for $200 < Re < 380$. Fluid Dyn. 41 (5) (2006) 795–809.
[11] J. Mittal, J.J. Wilson, F.M. Najjar, Symmetry properties of the transitional sphere wake. AIAA J. 40 (3) (2001) 579–582.
[12] Kim, S. Elghobashi, W. Sirignano, Three-dimensional flow over two spheres placed side by side. J. Fluid Mech. 246 (1993) 465–488.
[13] R. Folkersma, H.N. Stein, F.N. van de Vosse, Hydrodynamic interactions between two identical spheres held fixed side by side in a uniform stream directed perpendicular to the line connecting the spheres' centres. Int. J. Multiphase Flow 26 (2000) 877–887.
[14] D. Brydon, M.C. Thompson, Flow interaction between two spheres at moderate Reynolds numbers, in: 14th Australasian Fluid Mech. Conf., Adelaide, Australia, Dec. 10–14 2001.
[15] L. Schouveiler, A. Brydon, T. Leweke, M.C. Thompson, Interactions of the wakes of two spheres placed side by side. Eur. J. Mech. B/Fluids 23 (2004) 137–145.
[16] J.-F. Zou, A.-L. Ren, J. Deng, Study on flow past two spheres in tandem arrangement using a local mesh refinement virtual boundary method. Int. J. Numer. Meth. Fluids 49 (2005) 465–488.
[17] P.J. Olsson, L. Fuchs, The interaction of spherical particles in a fluid flow governed by Navier–Stokes equations, in: ECCOMAS. John Wiley & Sons, Ltd., 1998, pp. 180–185.
[18] R.C. Chen, J.L. Wu, The flow characteristics between two interactive spheres. Chem. Eng. Sci. 55 (2000) 1143–1158.
[19] L. Prahl, A. Hölzer, D. Arlov, J. Revstedt, M. Sommerfeld, L. Fuchs, A study of the interaction between two fixed spherical particles. Int. J. Multiphase Flow 33 (2007) 707–725.
[20] R.C. Chen, Y.N. Lu, The flow characteristics of an interactive particle at low Reynolds numbers. Int. J. Multiphase Flow 25 (1999) 1645–1655.
[21] T. Tsuji, R. Narutomi, T. Yokomine, S. Ebara, A. Shimizu, Unsteady three-dimensional simulation of interactions between flow and two particles. Int. J. Multiphase Flow 29 (2003) 1431–1450.
[22] S.-C. Liang, T. Hong, L.-S. Fan, Effects of particle arrangements on the drag force of a particle in the intermediate flow regime. Int. J. Multiphase Flow 22 (2) (1996) 285–306.
[23] C. Zhu, S.-C. Liang, L.-S. Fan, Particle wake effects on the drag force of an interactive particle. Int. J. Multiphase Flow 20 (1) (1994) 117–129.
[24] J. Gullbrand, X.-S. Bai, L. Fuchs, High-order Cartesian grid method for calculation of incompressible turbulent flows. Int. J. Numer. Meth. Fluids 36 (2001) 687–709.
[25] L. Fuchs, H.-S. Zhao, Solution of three-dimensional viscous incompressible flows by a multi-grid method. Int. J. Numer. Meth. Fluids 4 (1984) 539–555.
[26] D. Lörstad, L. Fuchs, A volume of fluid (vof) method for handling solid objects using fixed Cartesian grids, in: Moving Boundaries VI – Computational Modelling of Free and Moving Boundary Problems. Wessex Inst. of Techn., 2001, pp. 143–152.
[27] M. Rudman, A volume-tracking method for incompressible multifluid flows with large density variations. Int. J. Numer. Meth. Fluids 28 (1998) 357–378.
[28] E.G. Puckett, A.S. Almgren, J.B. Bell, D.L. Marcus, W.J. Rider, A high-order projection method for tracking fluid interfaces in variable density incompressible flows. J. Comput. Phys. 130 (1997) 269–282.
[29] D. Lörstad, Numerical modeling of deforming bubble transport related to cavitating hydraulic turbines, PhD thesis, Lund University, Lund, Sweden, 2003.
[30] J. Jeong, F. Hussain, On the identification of a vortex. J. Fluid Mech. 285 (1995) 69–94.
[31] P. Ploumhans, G.S. Winckelmans, J.K. Salmon, A. Leonard, M.S. Warren, Vortex methods for direct numerical simulation of three-dimensional bluff body flows: application to the sphere at $Re = 300$, 500 and 1000. J. Comput. Phys. 178 (2002) 427–463.
[32] J. Revstedt, A virtual boundary method with improved computational efficiency using a multi-grid method. Int. J. Numer. Meth. Fluids 45 (7) (2004) 775–795.
[33] L. Prahl, J. Revstedt, L. Fuchs, Sphere wake dynamics, in: Proc. of the 2nd Int. Conf. on Jets, Wakes and Separated Flows, 2008.
[34] D.-H. Yoon, K.-S. Yang, Flow-induced forces on two nearby spheres. Phys. Fluids 19 (2007).